Optical Constants of Al_2O_3 Smoke in Propellant Flames

David L. Parry* and M. Quinn Brewster†
University of Illinois at Urbana-Champaign, Urbana, Illinois 61801

An in situ light scattering and extinction technique was developed to determine the optical constants ($n-ik$) and mean optical size (d_{32}) of molten Al_2O_3 smoke particles in propellant flames. Direct transmittance and bidirectional transmittance and reflectance measurements were made using scattered laser light on aluminimized solid propellant flames at visible and near infrared wavelengths ($\lambda_1 = 0.6328$ μm and $\lambda_2 = 1.064$ μm). The optical properties of the molten Al_2O_3 smoke combustion product were obtained from the light scattering and extinction measurements by inverse solution of the radiative transfer equation. A mean optical size of $d_{32} = 0.97$ μm was obtained, which agrees well with other reported values. The values of n obtained for molten Al_2O_3 at 2680 K ($n_{m,\lambda 1} = 1.65$ and $n_{m,\lambda 2} = 1.64$) were significantly less than the values which have been reported for solid Al_2O_3 at temperatures just below the melting point of 2320 K ($n_{s,\lambda 1} = 1.82$ and $n_{s,\lambda 2} = 1.81$) indicating that a substantial decrease in n occurs upon melting. This decrease in n can be attributed to the expansion that takes place upon melting and is in good qualitative agreement with the predictions of the Lorentz-Lorenz equation. The value of k obtained for molten Al_2O_3 at 2680 K was 0.006 ± 0.004 (at both wavelengths), which is in reasonable agreement with other reported values. A dispersion analysis was also performed to fit this and other data over the spectral region from 0.5 to 5.0 μm and for temperatures from 2320 to 3000 K.

Nomenclature

d = particle diameter, μm
f_v = particle volume fraction
H = effective wave number, μm^{-1}
I = intensity
k = absorption index
N = particle number density distribution
N_d = total particle number density, cm^{-3}
n = refractive index
p = scattering phase function
$<p>$ = scattering asymmetry factor
Q = efficiency
r = particle radius
T = temperature or direct transmittance, K
t = optical thickness
x = particle size parameter, $\pi d/\lambda$
α, β = particle size distribution parameters
γ = dispersion oscillator relaxation parameter, μm^{-1}
ϵ = dialectric constant
η = wave number
Θ = single scattering polar angle
θ = slab polar scattering angle
λ = wavelength
μ = $\cos\theta$
ρ = density or reflectivity
ρ'' = bidirectional reflectivity
σ = normalized standard deviation
τ'' = bidirectional transmissivity
ω_o = single scattering albedo

Subscripts

a = absorption
b = backward
e = extinction
f = forward
L = cell or flame thickness
m = molten
mp = most probable
o = center wave number
p = plasma
ref = reference cell
s = solid or scattering

Superscripts

$\bar{}$ = average over particle size
$'$ = real part
$''$ = imaginary part
$*$ = nondimensional

Received June 5, 1989; revision received July 20, 1989.

*Graduate Research Assistant, Department of Mechanical and Industrial Engineering.
†Associate Professor, Department of Mechanical and Industrial Engineering. Member AIAA.

Introduction

THE optical constants ($n-ik$) and particle size of molten Al_2O_3 are important in several areas of solid rocket motor analysis. In heat transfer analysis, these properties are necessary for predicting radiative heat transfer to the nozzle,[1] internal insulator surfaces,[2] external equipment,[3] and to the burning propellant surface itself.[4] In performance analysis, the size distribution of particles entering the nozzle is of interest because of the strong influence of nozzle two-phase flow losses on performance.[5] Although the optical properties of Al_2O_3 have been studied extensively in the past, there is still considerable uncertainty about what values to use in any given situation. Much of this uncertainty is a result of the fact that most previous measurements of these properties have been made either using samples other than actual particles produced by propellant combustion or under conditions different from the actual propellant product gas environment, such that the particle composition (i.e., purity and stoichiometry) is probably quite different from that which exists in the actual propellant product gas environment. In this paper, new measurements are reported for the optical constants of molten Al_2O_3 smoke particles produced by propellant combustion as well as their mean optical size (d_{32}). These measurements are based on a multiwavelength, in situ, inverse light scattering and extinction technique carried out in the actual propellant flame environment.

Solid Phase Optical Constants

The optical constants of Al_2O_3 in the pure solid state have been relatively well established by many previous investigations.[6-21] Figures 1 and 2 show that at room temperature, pure

Al_2O_3 is essentially nonabsorbing between 0.5 and 5 μm. Below 0.2 and above 6 μm, electronic transitions and lattice vibrations, respectively, result in photon absorption. The refractive index n_s varies between 1.8 and 1.6,[6] and the absorption index k_s varies betweeen 10^{-7} and 10^{-5} depending on wavelength.[7] Measurements at higher temperatures[8] indicate that n_s increases as temperature increases with a nearly constant coefficient, $2.9\times10^{-5}K^{-1}$,[9] as shown in Fig. 1. The absorption index also increases with increasing temperature,[8,10,18] as shown in Fig. 2. However, the data of Konopka et al.,[10] which were taken from measurements using actual rocket particles heated in a shock tube, as compared with Gryvnak's data for pure Al_2O_3, indicate that composition is an important factor in determining the absorption index as well as temperature. Other studies[23,24] also indicate that stoichiometry can significantly influence the value of k. Substoichiometric aluminum oxide (Al_2O_{3-x}) can appear grey or black even at room temperature in contrast to the normal white color of stoichiometric Al_2O_3.

Liquid Phase Optical Constants

The optical constants of Al_2O_3 in the molten state ($T_m = 2320$ K) have not been as well characterized as those for the solid state. Most studies indicate that k increases substantially upon melting with a bigger increase occurring in relatively pure and stoichiometric samples.[8,10,12,14,15] Figure 3 shows that most of the reported values of k_m between 0.5 and 5 μm are in the range of 10^{-3}–10^{-2}. Recently, Reed[16] suggested a relation for estimating k_m between 1.7 and 4.5 μm based on extinction and emission measurements using particles that were collected from a rocket plume and heated in a shock tube:

$$k_m = 3.7\times10^{-4}\cdot T(\mathrm{K})^{1.5}\cdot\lambda(\mu\mathrm{m})\cdot10^{-13{,}500/T(\mathrm{K})} \quad (1)$$

Predictions for k_m based on Eq. (1) are in reasonable agreement with other data plotted in Fig. 3; however, Eq. (1) does not extend to short enough wavelengths to predict the upswing in k_m due to electronic transitions in the long-wavelength tail of the fundamental electronic absorption edge.

Conspicuously absent from the literature are data for direct measurements of the refractive index of molten Al_2O_3. The data of Gal and Kirch[11] plotted in Fig. 1 at 3000 K are apparently a simple extrapolation based on solid phase data and not actual measuremnts. While this type of extrapolation has been widely used to estimate n_m,[10,11,14,15,19,22] it ignores the change in density that occurs upon melting and the accompanying change in refractive index which takes place. Although this approximation is reasonable for predicting emission and absorption properties, it is not reasonable for predicting scattering properties.

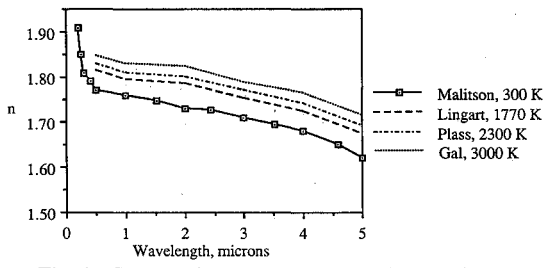

Fig. 1 Survey of aluminum oxide refractive index.

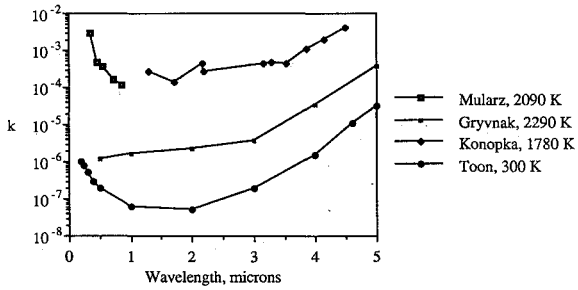

Fig. 2 Survey of solid aluminum oxide absorption index.

Particle Size Distribution

It is generally recognized that the particle size distribution of Al_2O_3 produced by combustion of aluminum is bimodal due to two competing oxidation mechanisms.[25-27] One mechanism is detached "vapor-phase" oxidation that produces submicron smoke, and the other is surface oxidation/condensation that produces large residual caps ($10-100$ μm). Due to their small size and large specific surface area, it is the smoke particles that dominate the optical properties of aluminized propellant flames and which are of primary interest in this study.

Both in situ optical techniques and particle collection techniques have been used to measure the size of combustion-generated particles such as Al_2O_3.[25-29] Although direct particle collection is generally considered to be more reliable, it is always accompanied by questions of possible biasing of the size distribution through the collection process itself. Optical techniques, on the other hand, can be carried out nonintrusively but are usually subject to limitations in the measurable size range ($\pi d/\lambda > 5$), the restriction of single scattering, and the need to know n and/or k independently.

Objective

Because of the uncertainty that still exists in the optical properties of Al_2O_3 in propellant flames, a light scattering and extinction technique was developed to determine simultaneously the optical constants and particle size of molten Al_2O_3 particles produced by aluminum combustion in solid propellant flames. An effort was made to overcome or at least mitigate several of the limiting aspects of previous studies of these properties. In that regard, measurements were made in situ using typical aluminized solid propellant formulations. Absolute scattering measurements were made, and multiple scattering was included in the data reduction by incorporating an inverse solution of the radiative transfer equation.

Light Scattering and Extinction Technique

Light scattering and extinction measurements were made using the experimental apparatus shown in Fig. 4. Two lasers, a 5-mW He-Ne laser ($\lambda_1 = 0.6328$ μm) and a 50-mW Nd-YAG laser ($\lambda_2 = 1.064$ μm) were used to obtain data at visible and near infrared wavelengths, respectively. A beam splitter cube was used to separate each laser beam into two parts. One path was used for bidirectional transmittance (forward scattering) measurements and the other for bidirection reflectance (backward scattering) measurements. Only one path and one laser beam were allowed to be incident on the flame zone at a time. Azimuthal angle dependence of the scattered light was eliminated by aligning the incident laser beam perpendicular to the flame zone. Light scattered in the forward direction was measured at approximately 11 deg from the normal to the flame

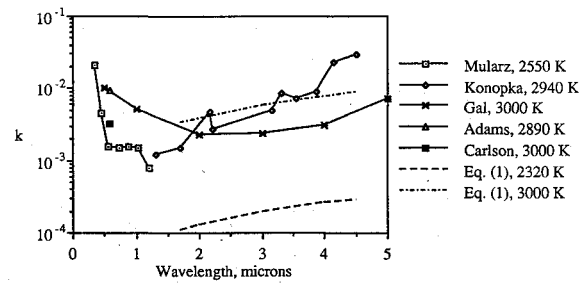

Fig. 3 Survey of molten aluminum oxide absorption index.

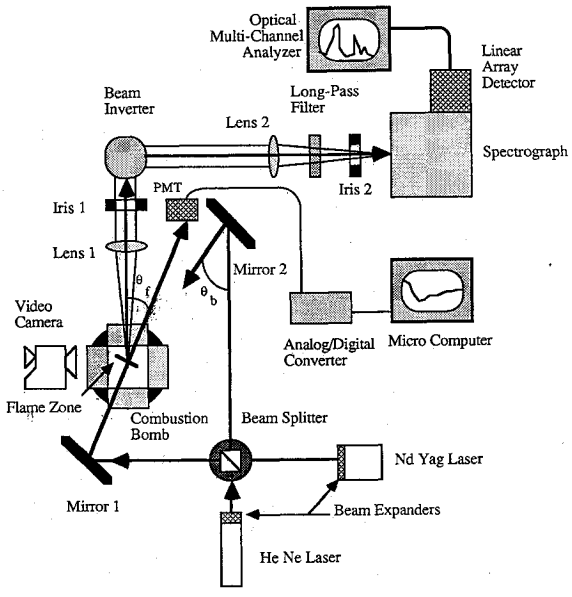

Fig. 4 Optical apparatus schematic diagram.

($\theta_f = 11$ deg) and light scattered in the backward direction at approximately 17 deg from the normal ($\theta_b = 17$ deg).

The optical system was set up and aligned to direct the scattered laser light to the entrance slit of the spectrograph. The vertical spectrograph entrance slit was imaged as a horizontal slit at the center of the flame zone by lenses 1 and 2 and a beam inverter. An optical multichannel analyzer with a linear diode array detector was used to measure the intensity of the scattered light I over a spectral region of interest (ROI) from 628 to 639 nm for the He-Ne signal and from 1059 to 1069 nm for the Nd-YAG signal. Background thermal emission from the flame was subtracted from the total signal giving a signal which was proportional to only the scattered light intensity.

A photomultipler tube (PMT) and a silocon diode detector (SDD) were used to detect the directly transmitted He-Ne and Nd-YAG laser light, respectively. Output voltages from the PMT and SDD corresponded to the direct, unscattered transmission T through the flame. The directly transmitted beams were also passed through narrow-band pass filters to prevent a significant amount of flame emission from reaching the PMT or SDD. The output signals of the PMT and SDD were processed by a microcomputer through an analog/digital converter. The computer was also used to trigger the ignition of the propellant with a nichrome wire and to trigger the scanning of the optical multichannel analyzer.

The combustion chamber was equipped with a nitrogen gas purge to exhaust the combustion products, to keep the windows clean, and to maintain the pressure in the combustion chamber at 1.8 MPa (250 psig). A video camera with a 1000 power neutral density filter was used to estimate the linear propellant burning rate (5 mm/s) and record the combustion process to allow rejection of abnormal propellant burns. Measurements were collected from a spatial region 4–7 mm above the burning propellant surface to ensure that sufficient aluminum combustion had occurred so that oxide smoke dominated the optical properties of the flame. The $1 \times 6 \times 15$ mm propellant strands consisted of 68% ammonium perchlorate (AP), 12% polymer binder (HTPB), and 20% aluminum (Al) by mass.

In order to make absolute scattering measurements (i.e., to obtain absolute intensity and not just intensity relative to some unknown reference intensity such as incident intensity or intensity at some other scattering angle), a reference measurement using a known reference intensity was required. A reference cell geometrically similar to the flame zone was used to obtain reference measurements for scattered intensity (I_{ref}) and direct transmission (T_{ref}) as shown in Fig. 5. The reference

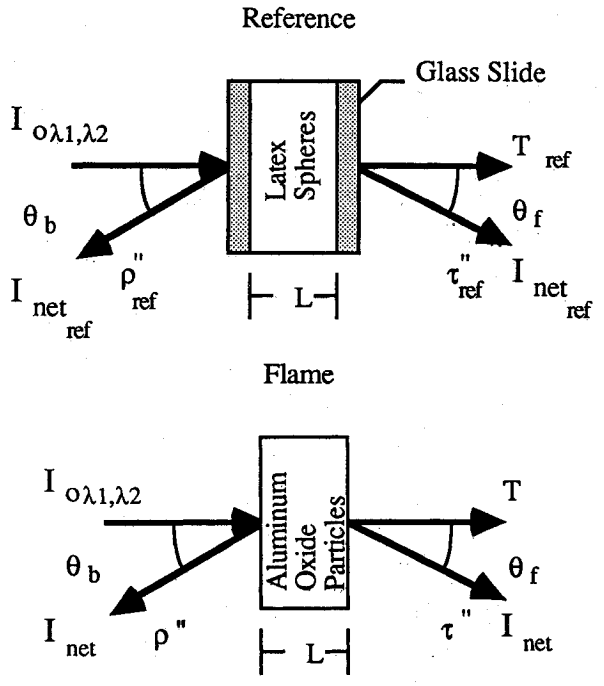

Fig. 5 One-dimensional planar scattering geometry for the experimental technique.

cell consisted of two glass slides (slab thickness $L = 1$ mm) filled with an aqueous suspension of polystyrene latex spheres (2% by mass). Latex spheres with a diameter of 107 ± 3 nm and 200 ± 6 nm were used for reference measurements at $\lambda_1 = 632.8$ nm and $\lambda_2 = 1.06$ nm, respectively. The refractive index of the latex particles was essentially the same (1.59) at both wavelengths.[30]

Scattering and Extinction Results

The results of the scattering and extinction measurements (optical thickness, bidirectional transmittance and bidirectional reflectance) are listed in Table 1 for both wavelengths.

The optical depth t_L was obtained for both the flame and reference cell from the direct transmittance measurements using Beer's law:

$$T = \exp(-t_L) \tag{2}$$

Bidirectional transmittance and reflectance for the reference cell, τ''_{ref} and ρ''_{ref}, were obtained from a discrete ordinate solution of the one-dimensional radiative transfer equation using as input parameters the measured optical thickness $t_{L\text{ref}}$, an albedo of $\omega_o = 1$, and a single scattering phase function calculated from Mie theory (essentially Rayleigh scattering). Since the aqueous solution used for the reference measurements was contained between glass slides, the effects of multiple reflection inside, outside, and between the glass slides as well as refraction and total internal reflection were included in both the determination of T_{ref} and in the transfer equation solution for τ''_{ref} and ρ''_{ref}. Once the reference and experimental intensity values were measured (e.g., I_{ref} and I, respectively), τ'' and ρ'' were determined on a relative basis using Eqs. (3) and (4).

Forward:

$$\frac{\tau''}{\tau''_{\text{ref}}} = \left(\frac{I}{I_{\text{ref}}}\right)_{\text{trans}} \tag{3}$$

Backward:

$$\frac{\rho''}{\rho''_{\text{ref}}} = \left(\frac{I}{I_{\text{ref}}}\right)_{\text{ref 1}} \tag{4}$$

Table 1 Scattering and extinction results

Type	Wavelength, μm	t_L	τ''	ρ''
Polystyrene reference	$\lambda_1 = 0.6328$	1.78	0.40	0.43
Polystyrene reference	$\lambda_2 = 1.064$	1.89	0.42	0.43
Al_2O_3 in flame	$\lambda_1 = 0.6328$	1.28 ± 0.11	1.37 ± 0.07	0.13 ± 0.03
Al_2O_3 in flame	$\lambda_2 = 1.064$	1.21 ± 0.23	1.05 ± 0.06	0.13 ± 0.07

Table 1 shows that the flame bidirectional transmittance values were an order of magnitude larger than the reflectance values, which, given the value of optical depth (1.2), is an indication of strong forward scattering.

Inverse Solution for Optical Properties

An implicit method involving Mie scattering theory coupled with the radiative transfer equation was used to determine the effective optical constants (n and k) and the size distribution parameters of the Al_2O_3 smoke particles formed in the propellant flames. This method required that the particle size distribution and optical constants be assumed to obtain the Mie scattering parameters. These parameters were then used in a solution of the transfer equation to determine bidirectional transmittance and reflectance values. These calculated transmittance and reflectance values were then compared to the corresponding experimental values (Table 1). A solution (not necessarily unique) for the optical properties was obtained when the calculated values of τ'' and ρ'' were found to be equal to the corresponding measured values to within the experimental uncertainties at both wavelengths. By requiring the optical properties to also satisfy the two spectral extinction measurements and a simple dispersion relationship, it was possible to find only one solution region of the system of equations. Although this does not constitute a mathematical proof of uniqueness, the fact that the solution was in good agreement with other reported values gives confidence that the solution found was the correct solution.

Particle Size Distribution

A monomodal gamma function size distribution was assumed to represent the Al_2O_3 particle sizes:

$$N(r) = \frac{N_d \beta^{\alpha+1}}{\Gamma(\alpha+1)} r^{\alpha} \exp(-\beta r) \tag{5}$$

where α and β are parameters describing the distribution, and $N(r)$ is the number density of specified particle radius r. A monomodal representation is adequate if one mode dominates the optical properties. In the present investigation, the Al_2O_3 smoke particles were assumed to dominate the optical scattering and extinction characteristics of the flame. (This assumption was verified by taking high-speed photographs of the region 4–7 mm above the surface of the burning propellant where measurements were made.) This distribution can also be characterized by the optical mean size d_{32}:

$$d_{32} = \frac{2(3+\alpha)}{\beta} = 2\frac{\int_0^\infty r^3 N(r)\,dr}{\int_0^\infty r^3 N(r)\,dr} \tag{6}$$

and most probable size d_{mp} (size where $dN/dr = 0$)

$$d_{mp} = 2\alpha/\beta \tag{7}$$

the parameter d_{32} is a mean optical size which can be regarded as the location parameter of the distribution, and d_{mp}/d_{32} can be regarded as the width parameter with an upper limit of 1 for a monodispersion and a lower limit of 0 for an infinitely wide polydispersion. The significance of using d_{32} is that for relatively large particles and realistic size distributions, which are wide enough to integrate out the interference oscillations in the monodisperse Mie parameters, the size-averaged Mie parameters [$(\bar{Q}_{a,s,e}, \bar{\omega}_o$, and $\bar{p}(\Theta)$] are independent of the width parameter d_{mp}/d_{32}. Assuming the smoke particles in this study satisfy these requirements ($x_{32} = \pi d_{32}/\lambda > 1$ and $d_{mp}/d_{32} < 0.3$), the present characterization of the size distribution in terms of d_{32} simplifies the inverse solution problem significantly by eliminating the dependence of the measured quantities on the width of the size distribution.

Mie Scattering Parameters

The equations used for calculating the Mie scattering parameters for the polydispersion (indicated by an overbar) are summarized below. The absorption (a), scattering (s), and extinction (e) efficiencies are given by

$$\bar{Q}_{a,s,e} = \frac{\int_0^\infty Q_{a,s,e} r^2 N(r)\,dr}{\int_0^\infty r^2 N(r)\,dr} \tag{8}$$

the albedo $\bar{\omega}_o$ is given by

$$\bar{\omega}_o = \frac{\bar{Q}_s}{\bar{Q}_a + \bar{Q}_s} = \frac{\bar{Q}_s}{\bar{Q}_e} \tag{9}$$

and the phase function $\bar{p}(\Theta)$ is given by

$$\bar{p}(\Theta) = \frac{\int_0^\infty p(\Theta) Q_s r^2 N(r)\,dr}{\int_0^\infty Q_s r^2 N(r)\,dr} \tag{10}$$

The scattering asymmetry is often expressed in terms of the asymmetry factor $<\bar{p}>$, which is a measure of the relative forward-to-backward scattering ratio. The value of $<\bar{p}>$ ranges from -1 for maximum backward scattering to 1 for maximum forward scattering:

$$<\bar{p}> = \frac{1}{2}\int_{-1}^{1} \bar{p}(\Theta)\cos\Theta\,d(\cos\Theta) \tag{11}$$

The functional dependence of the Mie scattering parameters can be expressed as shown in Eqs. (12–14):

$$\bar{Q}_{a,s,e} = \bar{Q}_{a,s,e}(n, k, x_{32}, x_{mp}/x_{32}) \tag{12}$$

$$\bar{\omega}_o = \bar{\omega}_o(n, k, x_{32}, x_{mp}/x_{32}) \tag{13}$$

$$\bar{p}(\Theta) = \bar{p}(\Theta, n, k, x_{32}, x_{mp}/x_{32}) \tag{14}$$

where the effective size parameters based on the optical mean and most probable diameters are given by

$$x_{32,mp} = \pi d_{32,mp}/\lambda \tag{15}$$

Equations (12–14) express the Mie scattering parameters as functions of the optical constants and the particle size parameters. The Mie parameters were used to determine the bidirectional transmittance and reflectance τ'' and ρ'' from the solution of the radiative transfer equation as discussed in the following section.

Radiative Transfer Equation

The radiative transfer equation for a nonemitting, one-dimensional, plane parallel slab is

$$\mu \frac{dI}{dt} = -I + (\bar{\omega}_o/2)\int_{-1}^{1} I\bar{p}(\mu,\mu')\,d\mu' \tag{16}$$

where I is the spectral scattered intensity, μ is the cosine of the slab polar angle, θ ($0<\theta_f<\pi/2$ and $\pi/2<\theta_b<\pi$), and t is the optical depth. Equation (16) was solved by the discrete ordinate method with 20 discrete ordinates. The solution of Eq. (16) can be expressed functionally by Eqs. (17) and (18):

$$\tau'' = \tau''\left[\theta_f, t_L, \bar{\omega}_o, \bar{p}(\Theta)\right] \tag{17}$$

$$\rho'' = \rho''\left[\theta_b, t_L, \bar{\omega}_o, \bar{p}(\Theta)\right] \tag{18}$$

where

$$t_L = \frac{1.5 f_v L \bar{Q}_e}{d_{32}} \tag{19}$$

The functional relations used to solve for the particle optical properties can be obtained by substituting Eqs. (12–14) into Eqs. (17–19), giving

$$\tau''_{\lambda 1} = \tau''_{\lambda 1}(n_{\lambda 1}, k_{\lambda 1}, d_{32}, d_{mp}/d_{32}) \tag{20}$$

$$\tau''_{\lambda 2} = \tau''_{\lambda 2}(n_{\lambda 2}, k_{\lambda 2}, d_{32}, d_{mp}/d_{32}) \tag{21}$$

$$\rho''_{\lambda 1} = \rho''_{\lambda 1}(n_{\lambda 1}, k_{\lambda 1}, d_{32}, d_{mp}/d_{32}) \tag{22}$$

$$\rho''_{\lambda 2} = \rho''_{\lambda 2}(n_{\lambda 2}, k_{\lambda 2}, d_{32}, d_{mp}/d_{32}) \tag{23}$$

for specified scattering directions θ_f and θ_b. Since the volume fraction of the ensemble of particles is unknown, f_v is eliminated by taking the ratio of optical thickness at the two wavelengths, giving

$$\frac{t_{L_{\lambda 1}}}{t_{L_{\lambda 2}}} = \frac{Q_{e_{\lambda 1}}(n_{\lambda 1}, k_{\lambda 1}, d_{32}, d_{mp}/d_{32})}{Q_{e_{\lambda 2}}(n_{\lambda 2}, k_{\lambda 2}, d_{32}, d_{mp}/d_{32})} \tag{24}$$

To obtain closure, the slope of n vs λ for molten Al_2O_3 was assumed to be constant and equal to that for solid Al_2O_3 in the interval $0.6328 \le \lambda \le 1.064$ μm:

$$n_{\lambda 1} - n_{\lambda 2} = -0.025(\lambda 1 - \lambda 2) \tag{25}$$

This assumption appears to be reasonable because the value of n in the visible and near infrared region is primarly determined by electronic transitions in the ultraviolet region. Although the number density of atoms undergoing electronic transitions would significantly decrease upon melting (this causing a decrease in the magnitude of n), the spectral location and strength of the transitions, which would presumably be unchanged, and thus the slope of n vs λ would be expected to be nearly the same in both phases over this narrow spectral region.

Results

Equations (20–25) represent six equations with six unknowns ($n_{\lambda 1}$, $n_{\lambda 2}$, $k_{\lambda 1}$, $k_{\lambda 2}$, d_{mp}, and d_{mp}/d_{32}). Solutions to these six equations were obtained by a direct search method. The ranges considered for each variable are listed in Table 2.

Table 2 Ranges considered for each unknown variable

Unknown variable	Range considered
n	1.40–1.85
k	1×10^{-5}–2×10^{-2}
d_{32}	0.1–2 μm
$(d_{mp}/d_{32}) = (x_{mp}/x_{32})$	0.05–1.0

The results of the direct search procedure are presented in Table 3. A range of possible sizes form $d_{32}=0.86$–1.08 μm satisfied the six equations within the experimental uncertainty. For each size there was a range of possible values for n, and for each n there was a range of possible values for k. Rather than present the full array of solutions, only the values which gave the best match (i.e., near the center of the uncertainty intervals) are listed in Table 3 (the full array of solutions is presented in Ref. 31). It should be noted that, within the experimental uncertainty, it was not possible to distinguish between values of k at the two wavelengths. Thus $k_{\lambda 1}$ and $k_{\lambda 2}$ are treated as a single value k. It was also found that for realistic (i.e., relatively wide) particle size distributions ($0.05 \le d_{mp}/d_{32} \le 0.3$) the results were insensitive to the value of d_{mp}/d_{32}. (A value of 0.15 was used just to carry out the particle size integrations.) With the loss of d_{mp}/d_{32} as an unknown it would appear that the system of equations would become overconstrained. However, it should also be noted that the uncertainty interval on the measured value of $\rho''_{\lambda 2}$ was so wide (see Table 1) as to make Eq. (23) a relatively nonconstraining equation in the system.

Table 3 Optical properties of Al_2O_3 smoke particles $T=2680$ K

Property	Value	Standard deviation
d_{32}, μm	0.97	0.11
$n_{m\lambda 1}$	1.65	0.03
$n_{m\lambda 2}$	1.64	0.03
$k_{m\lambda 1,\lambda 2}$	6×10^{-3}	4×10^{-3}
d_{mp}/d_{32}	0.15	0.10

One of the important results to point out is that the values of n_m obtained in this study are significantly less than the solid phase values at temperatures near the melting point. This result is in agreement with the reported density increase which occurs upon melting and is to be expected. It should be noted, however, that, in the absence of any measurements, it has been common practice[10,11,14,15,19,22] to estimate the values of n_m by extrapolating the values of n_s near the melting point using only the temperature variation observed in the solid phase. Although this procedure is probably valid within a single phase, it does not include the density change effect at the melting point and thus overestimates the value of n_m.

The value of k in Table 3 is consistent with comparable values (i.e., same wavelength, temperature, and flame environment) reported in other studies. The effective temperature of the particles was determined to be 2680 ± 50 K. This temperature was determined by two-color emission measurements.

The Mie scattering parameters which were determined as part of the solution procedure are listed in Table 4. The particle size parameter at both wavelengths is greater than one, which accounts for the insensitivity of the solution to the size distribution width parameter d_{mp}/d_{32}. The relatively large values of the asymmetry factor indicate that single scattering was predominantly in the forward direction as evidenced by the measured bidirectional transmittance reflectance values (see Table 1).

Dispersion Analysis

Using the present results together with selected data from other investigations, a dispersion analysis was carried out to obtain temperature-dependent dispersion parameters for molten Al_2O_3. According to classical dispersion theory,[32] the real (ϵ') and imaginary (ϵ'') parts of the complex dielectric function are given by

$$\epsilon' = 1 + \sum_{i}^{N_{\text{oscillators}}} \frac{\eta_{pi}^2(H_{oi}^2 - \eta^2)}{(H_{oi}^2 - \eta^2)^2 + \gamma_i^2 \eta^2} \tag{26}$$

$$\epsilon'' = 1 + \sum_{i}^{N_{\text{oscillators}}} \frac{\eta_{pi}^2 \gamma_i \eta}{(H_{oi}^2 - \eta^2)^2 + \gamma_i^2 \eta^2} \tag{27}$$

Table 4 Mie scattering parameters for Al_2O_3 smoke particles

Parameter	$\lambda 1 = 0.6328$ μm	$\lambda 2 = 1.064$ μm
Particle size parameter, x_{32}	4.82 ± 0.55	2.86 ± 0.33
Extinction efficiency, $\bar{Q}_e$	2.65 ± 0.14	2.90 ± 0.47
Albedo, $\bar{\omega}_o$	0.94 ± 0.04	0.97 ± 0.03
Asymmetry factor, $<\bar{p}>$	0.67 ± 0.07	0.69 ± 0.07

Table 5 Data used for dispersion analysis

Temperature, K	Wavelength, μm	n_m	Source	k_m	Source
2320	0.55	—	—	1.0×10^{-3}	Ref. 15
	0.725	—	—	8.0×10^{-4}	Ref. 15
	1.0	1.62	Eq. (32)	—	—
	1.7	—	—	1.1×10^{-4}	Eq. (1)
	2.0	1.60	Eq. (32)	—	—
	3.0	1.59	Eq. (32)	—	—
	3.1	—	—	2.0×10^{-4}	Eq. (1)
	4.0	1.57	Eq. (32)	—	—
	4.5	—	—	2.9×10^{-4}	Eq. (1)
	5.0	1.54	Eq. (32)	—	—
2680	0.6328	1.65	Table 3	6.0×10^{-3}	Table 3
	1.064	1.64	Table 3	6.0×10^{-3}	Table 3
	1.7	—	—	8.3×10^{-4}	Eq. (1)
	3.0	1.61	Eq. (34)	—	—
	3.1	—	—	1.5×10^{-3}	Eq. (1)
	4.0	1.59	Eq. (34)	—	—
	4.5	—	—	2.2×10^{-3}	Eq. (1)
	5.0	1.56	Eq. (34)	—	—
3000	0.5	1.69	Eq. (34)	1.0×10^{-2}	Ref. 11
	1.0	1.66	Eq. (34)	5.2×10^{-2}	Ref. 11
	2.0	1.64	Eq. (34)	2.3×10^{-3}	Ref. 11
	3.0	1.63	Eq. (34)	2.4×10^{-3}	Ref. 11
	4.0	1.61	Eq. (34)	3.1×10^{-3}	Ref. 11
	5.0	1.58	Eq. (34)	4.5×10^{-3}	Ref. 11

Table 6 Plass' data for solid Al_2O_3 at 2300 K

λ, μm	0.5	1.0	2.0	3.0	4.0	5.0
n_s	1.83	1.81	1.80	1.77	1.74	1.69

where

$$\epsilon' = n^2 - k^2 \qquad \epsilon'' = 2nk \tag{28}$$

$$n = \frac{\sqrt{\epsilon'^2+\epsilon''^2}+\epsilon'}{2} \qquad k = \frac{\sqrt{\epsilon'^2+\epsilon''^2}-\epsilon'}{2} = \frac{\epsilon''}{2n} \tag{29}$$

In these equations, each of the oscillators is described by its plasma wave number η_{pi}, its damping coefficient γ_i, and its effective wave number H_{oi}. The effective wave number takes the induced field effect into account and retains the classical form of the dispersion equations. The effective wave number is determined from the characteristic wave number η_{oi} and the plasma wave number according to Ref. 33 as

$$H_{oi}^2 = \eta_{oi}^2 - (\eta_{pi}^2/3) \tag{30}$$

In the region of interest (0.5–5 μm), the optical constants can be satisfactorily fit by using just two oscillators, one in the ultraviolet (H_{o1}) accounting for electronic transitions and one in the infrared (H_{o2}) accounting for molecular vibrations. Since both oscillators are located outside the region of interest, the approximations $H_{o1} \gg \eta \gg H_{o2}$ and $k \ll n$ can be applied to Eq. (26), giving

$$\frac{n^2-1}{n^2+2} = \frac{\eta_{p1}^2}{3\eta_{o1}^2} \tag{31}$$

By definition, the plasma wave number squared is proportional to the number density of oscillators and therefore to the material density. Thus Eq. (31) can also be expressed as

$$\frac{n_m^2-1}{(n_m^2+2)\rho_m} = \frac{n_s^2-1}{(n_s^2+2)\rho_s} \tag{32}$$

which is the Lorentz-Lorenz relation. This relation can be used to estimate the change in refractive index, which occurs upon melting, if the density change is known.

A combination of data for n and k from this and other studies was used to fit the dispersion parameters. Data was used for three temperatures, 2320, 2680, and 3000 K, covering the spectral region from 0.5 to 5 μm. The data used for the dispersion analysis are listed in Table 5. The values of n_m at 2320 K were estimated using Eq. (32) and Plass' predictions for n_s at 2300 K as shown in Table 6. The density of solid Al_2O_3 at 2300 K was taken as $\rho_s = 3.73$ g/cm^3, and the density of molten Al_2O_3 at 2320 K was taken as $\rho_m = 3.02$ g/cm^3. The latter value is based on the results of Kirshenbaum and Cahill,[34] who give the following relation for the density of molten Al_2O_3 as a function of temperature, T(K):

$$\rho_m = 5.632 - 1.127\times10^{-3}T(\mathrm{K}),\ \mathrm{g/cm^3} \tag{33}$$

The values of n_m at 2680 K (at wavelengths other than 0.6328 and 1.06 μm) and at 3000 K were extrapolated from the values of n_m at 2320 K using a temperature coefficient:

$$dn_m/dT = 5.87\times10^{-5} \text{ per K} \tag{34}$$

which was based on a linear curve fit between the experimental values of n_m at 2680 K (0.6328 and 1.06 μm) and the values predicted by the Lorentz-Lorenz relation at 2320 K.

The dispersion parameters were determined by minimizing the function F, which is a measure of the error or difference between the theoretical and experimental values:

$$F = \sqrt{\sum_{j=1}^{N}\left(\frac{n_{ej}-n_{dj}}{n_{ej}}\right)2} + \frac{\sigma_n}{\sigma_k}\sqrt{\sum_{j=1}^{K}\left(\frac{k_{ej}-k_{dj}}{k_{ej}}\right)2} \tag{35}$$

Table 7 Dispersion parameters for two oscillators at three temperatures

Parameter	2320 K	2680 K	3000 K
$\eta_{p1}^2\left(\frac{1}{\mu m^2}\right)$	8.513×10^{1}	8.723×10^{1}	8.934×10^{1}
$\eta_{p2}^2\left(\frac{1}{\mu m^2}\right)$	8.915×10^{-3}	8.806×10^{-3}	8.839×10^{-3}
$\gamma_1^2\left(\frac{1}{\mu m^2}\right)$	6.783×10^{-4}	3.423×10^{-2}	1.995×10^{-1}
$\gamma_2^2\left(\frac{1}{\mu m^2}\right)$	8.630×10^{-7}	5.344×10^{-5}	1.088×10^{-4}

Table 8 Temperature coefficients for dispersion parameters

Ψ	a_0	a_1	a_2	a_3	a_4
η_{p1}^2	8.509×10^{1}	4.205	0	0	0
η_{p2}^2	8.853×10^{-3}	0	0	0	0
γ_1^2	7.450×10^{-4}	1.838×10^{-1}	8.626×10^{-1}	1.698	-8.195×10^{-1}
γ_2^2	8.630×10^{-7}	8.691×10^{-5}	1.832×10^{-5}	0	0

Table 9 Dispersion analysis results

Temperature, K	Wavelength, μm	n_m	k_m
2320	0.5	1.65	5.81×10^{-4}
	1.0	1.62	2.65×10^{-4}
	2.0	1.60	1.50×10^{-4}
	3.0	1.59	1.57×10^{-4}
	4.0	1.57	2.35×10^{-4}
	5.0	1.54	3.92×10^{-4}
2500	0.5	1.66	2.79×10^{-3}
	1.0	1.63	1.27×10^{-3}
	2.0	1.61	7.30×10^{-4}
	3.0	1.60	7.96×10^{-4}
	4.0	1.58	1.23×10^{-3}
	5.0	1.55	2.09×10^{-3}
2680	0.5	1.67	4.65×10^{-3}
	1.0	1.64	2.12×10^{-3}
	2.0	1.62	1.19×10^{-3}
	3.0	1.61	1.23×10^{-3}
	4.0	1.59	1.83×10^{-3}
	5.0	1.56	3.04×10^{-3}
2800	0.5	1.68	6.92×10^{-3}
	1.0	1.65	3.15×10^{-3}
	2.0	1.63	1.72×10^{-3}
	3.0	1.62	1.66×10^{-3}
	4.0	1.60	2.31×10^{-3}
	5.0	1.57	3.69×10^{-3}
3000	0.5	1.69	1.03×10^{-2}
	1.0	1.66	4.69×10^{-3}
	2.0	1.64	2.51×10^{-3}
	3.0	1.63	2.30×10^{-3}
	4.0	1.61	3.01×10^{-3}
	5.0	1.58	4.63×10^{-3}

The experimental values of n and k (from Table 5) are denoted by a subscript e, and the theoretical values predicted by the dispersion analysis are denoted by a d. The difference in the experimental uncertainty between n and k was accounted for by including the ratio of the normalized standard deviation of n, σ_n to the standard deviation of k, σ_k. The normalized standard deviations used throughout this analysis were based on the experimental uncertainty reported in Table 3 for n and k. The greater uncertainty for k was reflected in σ_n and σ_k, where $\sigma_n = 1.8\%$ and $\sigma_k = 67\%$ were used. The results of fitting the data of Table 5 to Eqs. (26) and (27) by minimizing Eq. (35) are presented in Table 7.

The characteristic wavelengths of the two oscillators were assumed to be $\lambda_{o1} = 0.1107$ μm in the ultraviolet region and $\lambda_{o2} = 17.57$ μm in the infrared region, based on previous dispersion analysis of solid Al_2O_3.[6,7,20,21] The characteristic wavelength in the ultraviolet region corresponds to electronic transitions and would be expected to be similar in both solid and liquid phases. The characteristic wavelength in the infrared region accounts for molecular and intermolecular vibrations (e.g., lattice vibrations for the solid phase) and therefore would be expected to change in passing from solid to liquid. Since the intermolecular restoring forces of the liquid are expected to be less than those in the solid, the characteristic wavelength in the liquid might be expected to be greater than 17.57 μm. However, it is difficult to estimate a more appropriate value fo λ_{o2}, due to the lack of radiative property measurements at longer wavelengths. Thus, for simplicity, the value of 17.57 was used. This assumption is of little importance in the spectral region of interest since the curve fit in this region is largely unaffected by the exact choice of the infrared oscillator wavelength outside the region of interest.

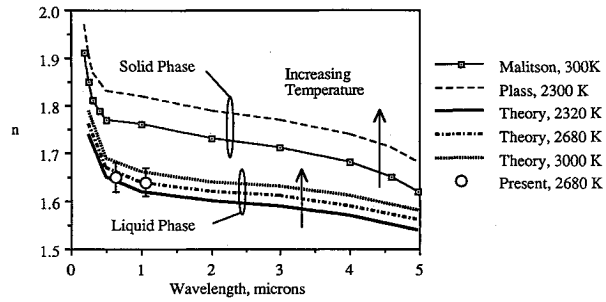

Fig. 6 Aluminum oxide refractive index (recommended).

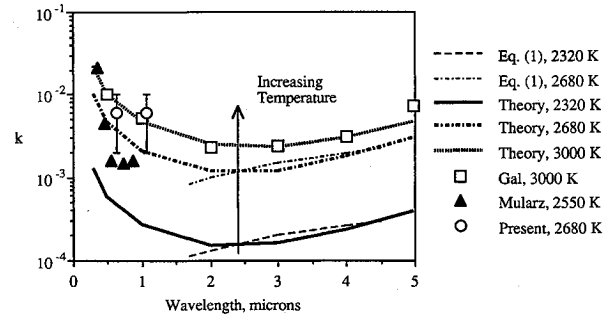

Fig. 7 Molten aluminum oxide absorption index (recommended).

The temperature dependence of the dispersion parameters was incorporated using a standard least-square curve fitting technique. The three values of each parameter were fit to a polynomial of sufficient degree to adequately represent the variation with temperature. The temperature was nondimensionalized according to

$$T^* = \frac{T - 2320\ \text{K}}{2000\ \text{K} - 2320\ \text{K}} \tag{36}$$

The polynomial equation used for a general dispersion parameter ψ was

$$\psi = a_0 + a_1 T^* + a_2 T^{*2} + a_3 T^{*3} + a_4 T^{*4} \tag{37}$$

with T in Kelvin. The coefficients that best fit the dispersion parameters are listed in Table 8. The values of n_m and k_m can be calculated for wavelengths between 0.5 and 5 μm and temperatures between 2320 and 3000 K by using the coefficients from Table 8 and Eqs. (26–37). Table 9 gives a list of n_m and k_m values that were determined using the results of the dispersion analysis.

The results for n_m and k_m from the dispersion analysis are plotted in Figs. 6 and 7 (labeled "theory") along with some of the values from Figs. 1–3 for comparison. The values of n_m are lower than the values for n_s at corresponding wavelengths, but both phases exhibit a positive temperature coefficient. The values of k_m also increase with temperature as expected.

Summary

The optical properties of molten Al_2O_3 smoke particles in a typical aluminized solid propellant flame were determined by

a light scattering and extinction technique. At 2680 K and 0.633–1.06 μm, results obtained were $n = 1.65$–1.64, $k = 0.006$, and $d_{32} = 0.97$ μm. The value of n showed a significant decrease upon melting attributable to the density change of Al_2O_3. The value of k was in reasonable agreement with other reported values, considering how sensitive k is to impurity and stoichiometry effects and the high level of uncertainty associated with these effects. The results obtained were combined with data from other investigators to determine temperature dependent dispersion parameters for molten Al_2O_3. More effort is still needed, however, to characterize the important effects of composition (i.e., stoichiometry and impurity) on the value of the absorption index.

Acknowledgments

Support for this work from Hercules, Inc. and the Astronautics Laboratory (Air Force Systems Command) (Contract F04611-86-C-0016), the National Science Foundation (Grant CBT 86-96162), and the Office of Naval Research (Contract N00014-87-K-0547) is gratefully acknowledged.

References

[1]Pearce, B. E., "Radiative Heat Transfer within a Solid-Propellant Rocket Motor," *Journal of Spacecraft and Rockets,* Vol. 15, No. 6, 1979, pp. 125–128.

[2]Brewster, M. Q., "Radiation-Stagnation Flow Model of Aluminimized Solid Rocket Motor Internal Insulator Heat Transfer," *Journal of Thermophysics and Heat Transfer,* Vol. 3, No. 2, 1989, pp. 132–139.

[3]Edwards, D. K., and Bobco, R. P., "Effect of Particle Size Distribution on the Radiosity of Solid Propellant Rocket Motor Plumes," AIAA Paper 81-1032, June 1981.

[4]Hardt, B. E., and Brewster, M. Q., "Influence of Metal Heat Feedback on Composite Solid Propellant Burning Rate," *Journal of Propulsion and Power* (to be published).

[5]Hermsen, R. W., "Aluminum Oxide Particle Size for Solid Rocket Motor Performance Prediction," *Journal of Spacecraft and Rockets,* Vol. 18, Nov.-Dec. 1981, pp. 483–490.

[6]Malitson, I. H., "Refracton and Dispersion of Synthetic Sapphire," *Journal of Optical Society of America,* Vol. 52, No. 12, pp. 1377–1379.

[7]Toon, O. B., and Pollack, J. B., "The Optical Constants of Several Atmospheric Aerosol Species: Ammonium Sulfate, Aluminum Oxide, and Sodium Chloride," *Journal of Geophysical Research,* Vol. 81, No. 33, Nov. 1976, pp. 5733–5748.

[8]Gryvnak, D. A., and Burch, D. E., "Optical and Infrared Properties of Al_2O_3 at Elevated Temperatures," *Journal of the Optical Society of America,* Vol. 55, No. 6, 1965, pp. 625–629.

[9]Plass, G. N., "Temperature Dependence of the Mie Scattering and Absorption Cross Sections for Aluminum Oxide," *Applied Optics,* Vol. 4, No. 12, 1965, pp. 1616–1619.

[10]Konopka, W. L., Reed, R. A., and Calia, V. S., "Measurements of Infrared Optical Properties of Al_2O_3 Rocket Particles," *Progress In Astronautics and Aeronautics,* Vol. 91, AIAA, New York, 1984, pp. 180–197.

[11]Gal, G., and Kirch, H., "Particulate Optical Properties in Rocket Plumes," AFRPL-TR-73-99, 1973, pp. 28–29.

[12]Carlson, D. J., "Emittance of Condensed Oxides in Solid Propellant Combustion Products," *Tenth (International) Symposium on Combustion,* The Combustion Institute, Pittsburgh, PA, 1965, pp. 1413–1424.

[13]Bauer, E., and Carlson, D. J., "Mie Scattering Calculations for Micron Size Alumina and Magnesia Spheres," *Journal of Quantitative Spectroscopy and Radiative Transfer,* Vol. 4, 1964, pp. 363–374.

[14]Adams, J. M., "A Determination of the Emissive Properties of a Cloud of Molten Alumina Particles," *Journal of Quantitative Spectroscopy and Radiative Transfer,* Vol. 7, 1967, pp. 273–277.

[15]Mularz, E. J., and Yuen, M. C., "An Experimental Investigation of Radiative Properties of Aluminum Oxide Particles," *Journal of Quantitative Spectroscopy and Radiative Transfer,* Vol. 12, 1972, pp. 1553–1568.

[16]Reed, B., "Optical Properties for Liquid Al_2O_3," private communication, Arnold AFB, Tullahoma, TN, Feb. 1988.

[17]Lee, D. W., and Kingery, W. D., "Radiation Energy Transfer and Thermal Conductivity of Ceramic Oxides," *Journal of the American Ceramic Society,* Vol. 43, No. 11, 1960, pp. 595–607.

[18]Myers, V. H., Oro, A., and DeWitt, D. P., "A Method for Measuring Optical Properties of Semi-Transparent Materials at High Temperatures," *AIAA Journal,* Vol. 24, No. 2, 1986, pp. 321–326.

[19]Lingart, H. K., Petrov, V. A., and Tikhonova, A. A., "Optical Properties of Leucosapphire at High Temperatures," *Teplofizika Vysokikh Temperature,* Vol. 20, No. 5, 1982, pp. 872–880.

[20]Barker, A. S., Jr., "Infrared Lattice Vibrations and Dielectric Dispersion in Corundum," *Physical Review,* Vol. 132, No. 4, 1963, pp. 1474–1481.

[21]Goodwin, D. G., and Mitchner, M., "Infrared Optical Constants of Coal Slags: Dependence on Chemical Composition," *Journal of Thermophysics and Heat Transfer,* Vol. 3, No. 1, 1989, pp. 53–60.

[22]Pustovalov, V. K., and Bosbuchendo, D. S., "Heating, Evaporation and Combustion of a Solid Aerosol Particle in a Gas Exposed to Optical Radiation," *International Journal of Heat and Mass Transfer,* Vol. 32, No. 1, 1989, pp. 3–17.

[23]Nelson, L. S., and Richardson, N. L., "Effects of Oxygen and Argon Atmospheres on Pendant Drops of Aluminum Oxide Melted with Carbon Dioxide Laser Radiation," *High Temperature Science,* Vol. 5, 1973, pp. 138–154.

[24]Kraeutle, K. J., and Bradley, H. H., Jr., "Combustion of Aluminized Propellants: The Influence of Pressure and Propellant Composition on Formation of Aluminum Combustion Residue," *14th JANNAF Combustion Meeting,* CPIA Publications, Laurel, MD, Vol. 1, pp 209–219.

[25]Kraeutle, K. J., "Particle Size Analysis in Solid Propellant Combustion Research," *Progress in Astronautics and Aeronautics,* Vol. 53, AIAA New York, 1977, pp. 449–463.

[26]Salita, M., "Quench Bomb Investigation of Al_2O_3 Formation From Solid Rocket Propellants (Part II): Analysis of Data, *25th JANNAF Combustion Meeting,* CPIA Publications, Laurel, MD, Oct. 1988.

[27]Dobbins, R. A., and Strand, L. D., "A Comparison of Two Methods of Measuring Particle Size of Al_2O_3 Produced by a Small Rocket Motor," *AIAA Journal,* Vol. 8, No. 9, pp. 1544–1550.

[28]Orguc, S., Pruitt, T. E., Edwards, T. D., Youngborg, E. D., Powers, J. P., Netzer, D. W., "Measurements of Particulate Size in Solid Rocket Motors," *Proceedings of 1987 JANNAF Combustion Meeting,* CPIA Publications, Laurel, MD, 1987, pp. 165–182.

[29]Powell, E. A., Cassanova, R. A., Bankston, C. P., and Zinn, B. T., "Combustion-Generated Smoke Diagnostics by Means of Optical Measurement Techniques," *Progress in Astronautics and Aeronautics,* Vol. 53, AIAA, New York, 1977, pp. 449–463.

[30]Inagaki, T., Arakawa, E. T., Hamm, R. N., and Williams, M. W., "Optical properties of polystyrene from the near-infrared to the x-ray region and convergence of optical sum rules," *Physical Review,* Vol. 15, No. 6, 1977, pp. 3246–3253.

[31]Parry, D. L., "Radiative Heat Transfer from Aluminum Oxide in Solid Propellant Flames," Ph.D. Dissertation, Dept. of Mechanical Engineering, Univ. of Illinois, Urbana, IL, 1989.

[32]Bohren, C. F., and Huffman, D. R., *Absorption and Scattering of Light by Small Particles,* Wiley, New York, 1983, pp. 227–283.

[33]Slater, J. C., and Frank, N. H., *Electromagnetism,* Dover, New York, 1969, pp. 109–114.

[34]Kirshenbaum, A. D., and Cahill, J. A., "The Density of Liquid Aluminum Oxide," *Journal of Inorganic Nuclear Chemistry,* Vol. 14, 1960, pp. 283–287.